A Novel Supramolecular Organogel Nanotubular Template Approach for Conducting Nanomaterials

P. Anilkumar[†] and M. Jayakannan*[,‡]

Chemical Sciences & Technology Division, National Institute for Interdisciplinary Science and Technology, Thiruvananthapuram-695019, Kerala, India, and Department of Chemistry, Indian Institute of Science Education and Research (IISER), NCL Innovation Park, Dr. Homi Bhabha Road, Pune 411008, India

Received: September 18, 2009; Revised Manuscript Received: October 25, 2009

We report a unique supramolecular organogel template approach for conducting polyaniline nanomaterials. A novel organogel based on sulfonic acid dopant was designed and developed from renewable resource 3-pentadecyl phenol via ring-opening of 1,4-butane sultone. The amphiphilic dopant molecule formed thermoreversible supramolecular organogel in highly polar solvents like alcohols. The self-assembled fibril network morphology of the gel was confirmed by scanning electron microscopy (SEM) and atomic force microscopy. Transmission electron microscopy (TEM) revealed that the inner part of the fibrous gel is nanotubular with the pore diameter of ~75 nm. The organogel nanotubular morphology was retained even in the presence of aniline+dopant complex, and the aniline monomers occupied the hydrophobic nanopockets provided by the amphiphilic dopant. The chemical oxidative polymerization of the dopant+aniline organogel template produced well-defined polyaniline nanofibers. The polymerization was carried out at various temperatures to establish the role of the physical state and stability of the organogel on the morphology. The sulfonic acid molecule acts both as self-assembled molecular template for the synthesis of polymer nanomaterial as well as anionic counterpart for stabilizing the positively charged conducting polymer chains. The gel template played a pivotal role in directing polyaniline chains to form nanofibers and also manipulating the number of other properties such as conductivity, solubility, percent crystallinity, and solid-state ordering, etc. Temperature-dependent electrical conductivity measurements revealed that the nanomaterials showed typical linear ohmic behavior and also followed the 3-D VRH model at elevated temperatures.

Introduction

The facile synthetic approaches and tunable redox properties of conducting polyaniline have provided new applications in the fields of microelectronics, sensors, actuators, surface coatings, and advanced catalysts.[1] Efforts have been made over the past decade to fabricate and manipulate polyaniline nanostructures using hard or soft templates, emulsion, interfacial, seeding, and dilute polymerization methods, etc.[2] Among all of the methods, the soft template method based on organic molecules was found most promising.[3] Amphiphilic, block copolymer micelles, liquid crystals, and self-assembled peptide systems were documented as soft templates for polyaniline nanostructures.[4] Recently, we have developed water-soluble amphiphilic sulfonic acid derivatives from renewable resource cardanol and successfully utilized their cylindrical, spherical, and vesicular templates for producing conducting polyaniline and polypyrrole nanostructures.[5] Self-organized molecular gels are another class of molecular templates, and they have been utilized to tune the shape and size of the nanomaterials such as silica, titania, gold, and silver.[6] In the area of polyaniline nanomaterials, polyaniline gels were prepared by mixing the polyaniline emeraldine base (PANI-EB) with suitable dopants such as camphorsulfonic acid, dinonylnaphthalenedisulfonic acid, and dodecylbenzenesulfonic acid in dry or wet conditions.[7] These gels showed more mechanical flexibility, crystallinity, etc., as compared to their parent polymer. Few commercially available organogelators such as cholicacid+polyethylene glycol and hexadecyltrimethylammonium chloride were explored as templates for conducting polyaniline.[8] Most often, the removal of these organic gelator molecules during the isolation of nanomaterials induced instability in the polyaniline morphology.[8] Additionally, the presence of these gelator molecules behaves as insulating external matrix and hampers the conductivity and other electronic properties of the conducting nanomaterials. Therefore, the idea of developing a new sulfonic acid-based dopant-cum gelator molecule is very attractive because the same molecular system can act as both self-organized gel-template for polyaniline nanomaterials as well as anionic counterpart for stabilizing the positively charged conducting chains. This approach is very important because: (i) it provides a new synthetic approach for conducting nanomaterials based on self-templating molecular system, (ii) it is important to understand the mechanism of the gel-templated nanomaterials synthesis, and (iii) it provides the opportunity for studying the superiority of the nanomaterials synthesized by gel-template approach. To our knowledge, there is no report known in the literature on a self-gel-template dopant for polyaniline or other conducting nanomaterials.

The present investigation is emphasized to design and develop new dopant-cum-molecular gelator as novel soft templates for polyaniline nanostructures. We have cleverly designed a novel gelator-cum-dopant, 4-(3-pentadecylphenoxy) butane-1-sulfonic acid, from a renewable resource derivative, 3-pentadecylphenol, which is obtained from the cashew nut processing industry. The sulfonic acid derivative possesses typical amphiphilic geometry

* Corresponding author. Fax: 0091-20-25898022. E-mail: jayakannan@iiserpune.ac.in.
[†] National Institute for Interdisciplinary Science and Technology.
[‡] IISER.

10.1021/jp909016r
Published on Web 11/19/2009

with a hydrophobic long tail and a hydrophilic acid head. It produces stable organo-gel nanotube in various organic solvents such as ethanol, methanol, chloroform, and dimethylsulfoxide at room temperature. The addition of aniline monomer into the dopant nanotube results in the formation of filled nanotubular self-organization, which template for the polyaniline nanofibers. The effects of gelation temperature, concentration, and composition of the reactants on the gel mechanism of the gel-template-assisted nanomaterials growth were investigated. The nanomaterials were found highly soluble in polar solvents like DMSO, which further facilitate the structural characterization by ^{1}H NMR, FT-IR, and UV−vis studies. The morphology of the synthesized polyaniline was analyzed by SEM and TEM, and the optical and electronic properties of nanomaterials were determined by UV−vis and four-probe conductivity measurements. DSC and WXRD studies were utilized to study the thermo-reversible and solid-state ordering of the resultant nanomaterials. Variable-temperature electrical conductance measurements were carried out to study the influence of molecular gel-template on the electronic behavior of polyaniline nanomaterials. The detailed investigation revealed that the nanomaterials synthesized by the gel-template assisted process possessed superior conductivity, crystallinity, and solid-state ordering.

Experimental Procedures

Materials. 3-Pentadecyl phenol, ammonium persulfate (APS), 1,4-butane sultone, and potassium tertiary butoxide were purchased from Aldrich and used as such. Aniline (Aldrich) was double distilled and kept under nitrogen gas prior to use.

General Procedures. NMR analysis of the samples was carried out in a 500 MHz Bruker Avance ii NMR spectrometer at 30 °C. The purity of the compounds was determined by JEOL JSM600 fast atom bombardment (FAB) mass spectrometry. For scanning electron microscopy (SEM) measurements, samples were subjected for thin gold coating using a JEOL JFC-1200 fine coater and analyzed using a JEOL JSM- 5600 LV scanning electron microscope. Atomic force microscopy (AFM) images of thin gel films were recorded under ambient conditions using a NT-DMT Ntegra machine operating in the tapping mode regime. Samples for the AFM imaging were prepared by drop casting the ethanol solutions onto freshly cleaved mica. Transmission electron microscopy (TEM) images were recorded using a FEI Tecnai 30G^2 S Twin HRTEM instrument operating at 100 kV. Wide-angle X-ray diffractions of the finely powdered polymer samples were recorded by Philips Analytical diffractometer using Cu Kα emission. UV−vis spectra of the PANI in water were recorded using Perkin-Elmer Lambda-35 UV−vis spectrophotometer. Infrared spectra of the compounds were recorded using a Perkin-Elmer, spectrum one FTIR spectrophotometer in the range of 4000−400 cm^{-1}. For conductivity measurements, the polymer samples were pressed into a 10 mm diameter disk and analyzed using a Keithley 6881 programmable current source and 2128A nanovoltmeter instrument. Thermal analyses of the samples were performed with a DSC Q20 model (TA Instruments) differential scanning calorimetry (DSC) instrument under dry nitrogen, and the instrument was calibrated with indium standards.

Synthesis of 4-(3-Pentadecylphenoxy)butane-1-sulfonic Acid. 3-Petadecylphenol (10 g, 33 mmol) was added into a flask containing potassium tertiary butoxide (7.52 g, 66 mmol) in dry ethanol (100 mL). This solution was heated (60 °C) for 30 min under nitrogen atmosphere. The contents were cooled, and 1,4-butane sultone (9 g, 66 mmol) was added dropwise. The reaction was continued by refluxing the content for 40 h under nitrogen atmosphere. It was cooled, and the precipitated white solid mass was isolated by suction filtration. The white potassium salt of the product was suspended in water (40 mL) and acidified by 5 M HCl (25 mL) to get a white precipitate as sulfonic acid. The crude solid was purified by passing through a silica gel column using 20/80 v/v methanol/chloroform as eluent. Yield = 10.5 g (70%). Melting point = 78−84 °C. ^{1}H NMR ($CDCl_3$, 500 MHz) δ: 6.96 (b, 1H, Ar−H), 6.59 (m, 3H, Ar−H), 3.71 (d, 2H, Ar−O**C**$\mathbf{H_2}$), 2.89 (d, 2H, −**C**$\mathbf{H_2}$ −SO_3H), 2.45 (b, 2H, Ar−**C**$\mathbf{H_2}$), and 2.08 (33H, aliphatic). ^{13}C NMR (DMSO-d_6, 125 MHz) δ: 158.8, 143.9, 129.1, 120.3, 114.7, 111.7, 59.6, 65.1, 51.3, 39.8, 35.1, 31.4, 30.7, 28.6, 28.2, 22.9, and 14.9. FT-IR (KBr, cm^{-1}): 3544, 3479, 2916, 2853, 1618, 1579, 1471, 1445, 1298, 1246, 1183, 1061, 970, 869, 774, 749, 723, 690, 684, 621, 588, and 524. FAB-MS (MW 440.0): m/z = 463.2 (M^+Na).

TABLE 1: Yield, S/N Ratio, Morphology, Viscosity, and WXRD Data of Polyaniline Nanomaterials

sample	yield[a]	S/N[b] ratio	morphology[c]	η_{inh} (dL/g)[d]	WXRD peaks[e] d-spacing
P-30	43	45.6	fiber, ∼150 nm	0.31	24.1,13.5,5.2,4.7,4.3, 4.2,3.9,3.7,3.5,3.1
P-45	42	45.5	fiber, ∼75 nm	0.29	25.6,13.7,4.7,3.4,3.1
P-65	39	35.3	agglomerates	0.24	26.1,13.7,4.7,4.3,3.5

[a] For isolated product. [b] From elemental analysis. [c] From SEM images. [d] Measured using Ubbelohde viscometer in NMP at 30 °C. [e] From powder X-ray diffraction.

Synthesis of Polyaniline Nanomaterials. The synthesis of polyaniline is described in detail for **P-30**, and other samples were prepared following a similar procedure. The dopant (0.5 g, 1.1 mmol) was dissolved in dry ethanol (50 mL) in a 100 mL beaker by heating in a water bath and cooled to 30 °C to obtain a thick gel. To this gel was added distilled aniline (1 mL, 1.02 g, 11 mmol; [aniline]/[dopant] = 10), and it was heated to 75 °C in a water bath for 5 min. The solution was allowed to cool at room temperature for 1 h, which produced an opaque gel. Ammonium per sulfate solution (3.73 M, 5 mL) was slowly added on the top of the gel at 30 °C, and the polymerization was allowed to continue at 30 °C for 24 h without any disturbance. Green colored polyaniline solid was filtered and washed with distilled water and methanol several times until the filtrate became colorless. The solid product was dried in a vacuum oven at 60 °C for 48 h (0.01 m Hg). Yield = 0.65 g (43%). ^{1}H NMR (DMSO-d_6, 500 M Hz) δ: 7.46 (2H, Ar−H, PANI), 7.41 (2H, Ar−H, PANI), 7.14 (1H, Ar−H, dopant), 6.99, 7.11, 7.21 (1H, 1/1/1 triplet, −NH^+, PANI), 6.73 (3H, Ar−H, dopant), 5.86 (1H, −N−H, PANI), and 4.5−0.5 (39H, aliphatic-H, dopant). FT-IR (KBr, in cm^{-1}): 3449, 3228, 2920, 2850, 1570, 1494, 1298, 1254, 1153, 1038, 806, 693, 623, and 503.

The samples **P-45** and **P-65** were synthesized following a similar procedure at 45 and 65 °C, respectively. The yield and elemental analysis data (S/N ratio) are provided in Table 1 and the Supporting Information.

Results and Discussion

A novel amphiphilic surfactant gelator molecule 4-(3-pentadecylphenoxy) butane-1-sulfonic acid was synthesized by ring-opening of 1,4-butanesultone by 3-petadecyl phenol, which is a biowaste from the cashew nut processing industry (see Figure 1). The molecule was obtained as a white crystalline powder, and its structure was confirmed by NMR, FT-IR, and mass. The four protons in the aromatic ring appeared with characteristic splitting pattern at 7.16 and 6.74 ppm. The protons Ar−O**C**$\mathbf{H_2}$

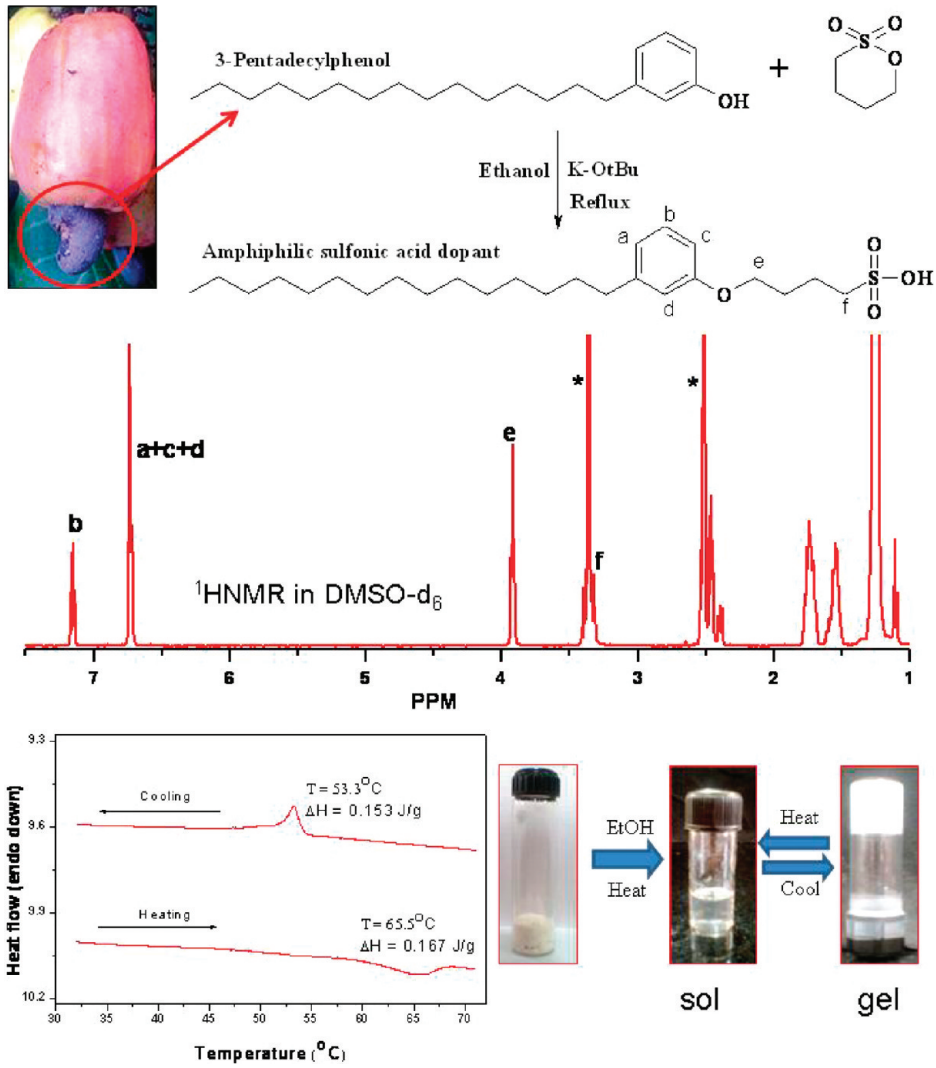

Figure 1. Synthesis, NMR spectrum (in d_6-DMSO), DSC analysis, and physical states of novel amphiphilic organogel dopant.

and CH_2-SO_3H appeared at 3.92 and 3.32 ppm, respectively. All other aliphatic protons appear below 3 ppm, and the intensities of the peaks matched with the expected structure. The new molecule possessed typical amphiphilic structure with a long flexible tail consisting of a pentadecyl chain and rigid polar hydrophilic head ($-SO_3H$). The amphiphilic dopant molecule was found to produce an opaque white gel in various organic solvents like ethanol, methanol, chloroform, DMSO, etc. Among all of the solvents, ethanol produced a stable gel morphology over a wide concentration range, and the organogel was stable for more than a month (see Figure 1). DSC analysis of the gel in ethanol showed a broad melting peak at 65 °C with respect to gel-to-sol transitions, and the sol-to-gel phase change occurred at 53 °C upon cooling. The gel was found to show reversible gel−sol transition in the repetitive heating/cooling process. Xerogels were subjected to various microscopic techniques such as SEM, AFM, and TEM, and the images are shown in Figure 2. The SEM image of the gel confirmed the presence of self-assembled long fibrillar tape morphology as a typical representation of organogels texture. The average diameters of the long tapes were found to be 150−350 nm with length up to 8−10 μm. AFM image (tapping mode) also supports the existence of gel network structure, and the tapes were entangled to produce 3D network structure. The average diameters of the fibrils were found as 200−300 nm and length up to 3 μm. TEM images revealed that the inner part of the fibrils was hollow, indicating that they were nanotubes of ~5 μm length. The average inner and outer diameters of the nanotubes were found to be 60 and 175 nm, respectively, and the wall thickness was in the range of 70 nm. The end-to-end distance of the amphiphilic molecule (via MM2 energy-minimized calculation) was found to be 2.7 nm, and so it is reasonable to believe that the nanotube is formed by a multilayer packing of dopants via layered self-assembly.

To transcribe the superstructures formed in the organogels into the conducting polyaniline structure, the dopant nanotubes were filled with aniline monomer and polymerized by standard chemical oxidative polymerization method. The amphiphilic dopant was heated to dissolve completely in ethanol and cooled to form gel. Aniline was added to this dopant gel and warmed to dissolve homogenously. Upon cooling, the dopant+aniline complex formed a stable self-assembled white gel (see Figure 3) similar to that of dopant alone (see Figure 1). The stability of the gel-template was checked for various composition of [aniline]/[dopant] from 5 to 20 (in moles), and it was found that homogeneous and stable gel was formed for an [aniline]/[dopant] ratio of 10. AFM analysis of the aniline+dopant gel template (see Figure 3) confirmed the existence of a uniform array of self-assembled bundles of fibrous network. TEM images of the dopant+aniline gel template also proved the presence of self-assembled nanotubes as similar to that of dopant gel (see Figure 2). The average diameters of the dopant+aniline nano-

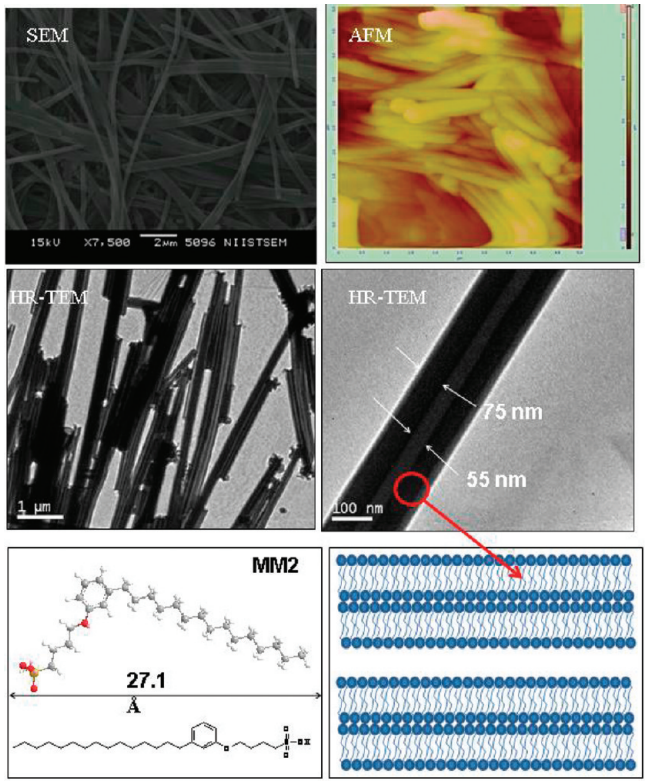

Figure 2. SEM, TEM, and AFM images of dopant gel (xerogel); MM2 structure of the dopant and schematic representation of multilayer nanotube.

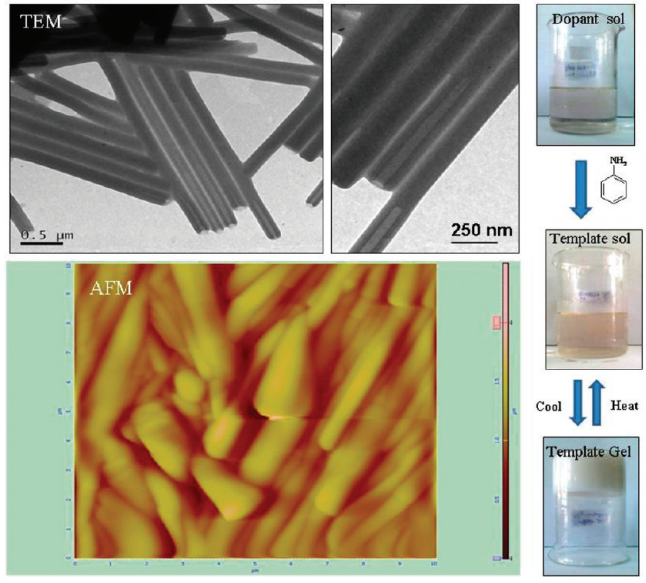

Figure 3. TEM and AFM images, and photographs of dopant+aniline gel template.

tubes were found to be 200 nm with length up to 4−5 μm. A close observation of the nanotubes revealed that the nanostructures were not hollow (unlike in the case of dopant gel; see Figure 2); rather, they were half-filled. The inner diameters of the dopant and dopant+aniline nanotubes were almost comparable. It suggests that during the gel formation the aniline monomers preferentially occupied the inner cavity of the nanotubes formed by the dopant molecules. FT-IR is an efficient tool to trace the hydrogen-bonding interactions between dopant and aniline molecules present in gel.[9] FT-IR spectra of dopant and dopant+aniline gels were recorded in chloroform solution

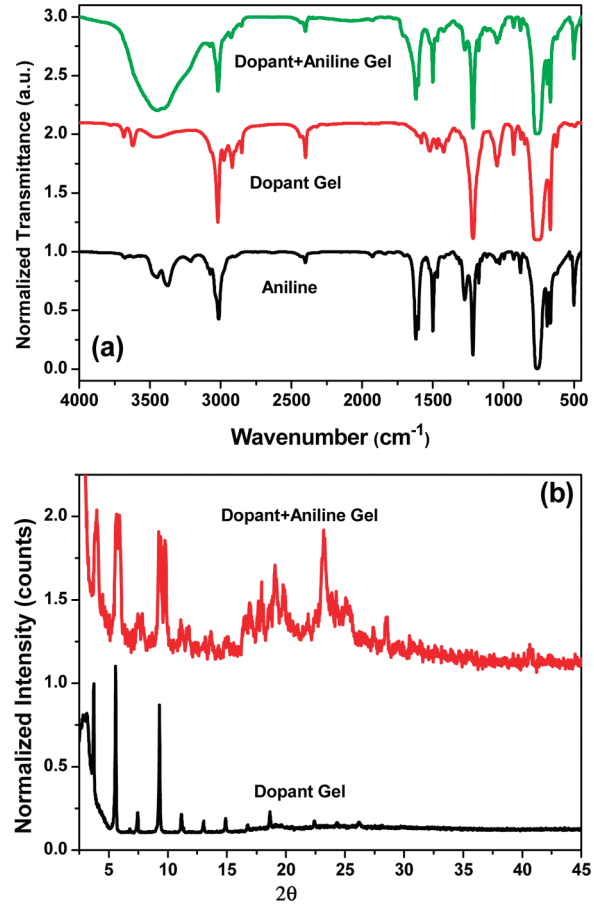

Figure 4. FT-IR and WXRD plots of the organo gels.

(1×10^{-3} M) (see Figure 4a). The spectrum of the dopant gel showed two peaks at higher wave numbers (3685 and 3619 cm^{-1}) with respect to antisymmetric and symmetric stretching vibrations of the O−H group in the sulfonic acid, respectively.[10] A broad peak was also seen at lower wavenumber (3460 cm^{-1}) corresponding to the hydrogen-bonded O−H stretching vibration. The FT-IR spectrum of aniline-dopant gel showed a broad peak at 3200−3600, indicating the presence of a strong hydrogen-bonding interaction between −NH and −OH groups of aniline and dopant molecules. To further confirm the aniline encapsulation and its effect on molecular packing, the gels were subjected to wide-angle X-ray diffraction (WXRD) studies (see Figure 4b). The self-assembled dopant showed a series of sharp reflections with the lower angle peak being the longest *d*-spacing of 31 Å (corresponds to $2\theta = 2.8°$).[11] The aniline-dopant gel showed all of the peaks observed in the parent dopant gel. Additionally, broad peaks were also noticed at a higher angle region in the dopant+aniline gel with *d*-spacing 4−3 Å (2θ = 16−26°), confirming the aromatic $\pi-\pi$ interaction among the dopant+aniline molecules.[12] The theoretical end-to-end distance of the dopant molecule (~2.7 nm = 27 Å; see Figure 2) was matching well with the *d*-spacing value of 31 Å in the WXRD pattern. It suggests that the dopant molecule exists in the form of layer-like self-assembly in the organo-gel nanotubes as shown in Figure 2. On the basis of the FT-IR and WXRD studies, it is believed that the dopant molecule self-assembled to form nanotubular gels in which the aniline molecules are stabilized via hydrogen-bonding or aromatic $\pi-\pi$ interaction.

The dopant+aniline gel template was oxidized by concentrated aqueous ammonium perdisulfate (APS) solution to produce conducting polyaniline nanomaterials. The influence

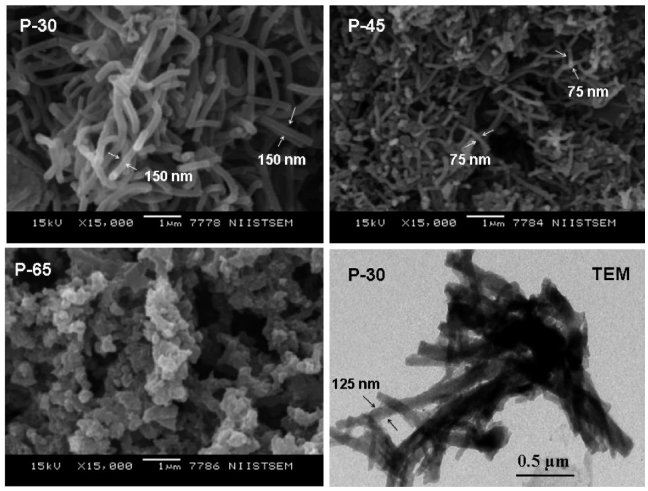

Figure 5. SEM and TEM images of polyaniline nanomaterials.

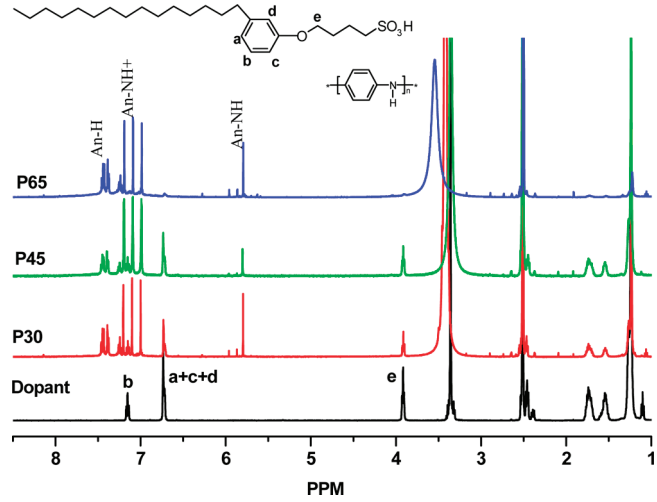

Figure 6. ^{1}H NMR spectra of polyaniline nanomaterials in d_6-DMSO.

of the physical state of gel on the morphology of the resulting conducting polymer was investigated by carrying out polymerization at three different temperatures. Two polymerizations were chosen in the gel state (below the gel-to-sol temperature at 30 and 45 °C) and one in the dissolved state of the molecules (65 °C, above gel-to-sol temperature). After the addition of APS solutions at the respective polymerization temperatures, the reaction proceeded for 24 h during which the entire reaction mixture transformed into a dark solid mass (snapshots of the gel-assisted polymerization process are in Figure 4 of the Supporting Information). At 30 °C, the dopant+aniline gel is very stable, and the added APS solution moved very slowly inside the self-assembled gel phase to oxidize the aniline monomer. The gel was found semirigid when the polymerization temperature was 45 °C, and the polymerization reaction (appearance of green color) occurred as soon as the oxidant solution was introduced. Polymerization at 65 °C (sol state) proceeded very fast as normally observed for polyaniline synthesis in aqueous or in organic solvents. The dark green powdered nanomaterial was filtered and washed well with distilled water followed by methanol until the filtrate became colorless. It was dried in a vacuum oven at 55 °C for 24 h prior to further analysis. The samples were denoted as **P-*X***, where ***X*** denotes the polymerization temperature.

The SEM images of **P-30** showed a mat of nanofibers with an average fiber diameter of ∼135 nm and length up to 5 μm long (see Figure 5). The sample **P-45** also showed thin nanofibers with average diameter of 75 nm with a length up to 3 μM. The sample synthesized at higher temperatures in sol-state (sample **P-65**) did not produce good morphology, and the image appeared as agglomerated particles. The TEM image of **P-30** showed the presence of a bundle of solid nanofibers of ∼100 nm diameter with 3 μm length. SEM and TEM analysis of the gel-templated polyaniline samples clearly indicated that the physical state of the supramolecular gel-assembly played a major role in determining the morphology of the resulting polymer nanostructure. In **P-30** and **P-45**, the self-assembled gel template produced uniform nanofibers, whereas at 65 °C when there was no self-assembled gel template, polymerization yielded agglomerated polyaniline. On the basis of the microscopic studies of the polyaniline nanofiber formed and gel template characterization by SEM, AFM, TEM, WXRD, and FT-IR, the following mechanism was proposed for polyaniline nanofiber synthesis via dopant molecular self-assembly in a gel state. The sulfonic acid dopant synthesized has a typical amphiphile structure and undergoes self-assembly in ethanol leading to the formation of open nanotubes with cavities of diameter ∼75 nm.[13] Upon gelation in the presence of aniline monomer, the amphiphiles will form nanotubes, and the aromatic aniline molecules will preferentially trap inside the hydrophobic regions of self-assembly and also tubular cavity due to the increased capillary action of nanodimensional cavities.[14] These nanoconfined aniline monomers on oxidation into polyaniline take the shape of the host cavity to produce nanofibers. Subsequent to the polymerization reactions, the amphiphilic sulfonic acid forms a strong complex with imine nitrogens of polyaniline and thereby acts as a dopant similar to any other sulfonic acid dopant. This in turn helped to arrest the nanofiber morphology in the network of gel.[7,15] This mechanism also underlines the fact that in the case of **P-65** sample the self-assembly of the template is not complete during oxidant addition because it is in the temperature range of gel melting (65 °C), and so the polymerization proceeds just like conventional polymerization in the presence of amphiphilic dopants, resulting in the formation of polyaniline with agglomerated morphology.

The long alkyl part of the amphiphilic molecule makes these conducting nanostructures soluble in highly polar solvents like DMSO for complete structural characterization by spectroscopic techniques. ^{1}H NMR spectra of the dopant and polyaniline nanomaterials were recorded in d_6-DMSO, and their spectra are shown in Figure 6. The aromatic protons appeared at 6.5−7.5 ppm, and all three polymer samples possessed almost identical splitting patterns.[16] The peaks in the 7.5−7.3 ppm region were assigned to protons of aromatic rings of polyaniline chains.[17] The three equally intense peaks (triplet) at 6.9, 7.1, and 7.2 ppm are attributed to the free radical NH proton resonance due to the ^{14}N with unit spin, which makes the proton attached to it split into three lines.[17] The spectra of the samples also have peaks corresponding to the dopant molecule in addition to their peaks, which confirmed the strong binding of sulfonic acid dopant to the polymer structure. The ratio of the peak integrals of the dopant (6.72/three protons) to polymer (7.39 and 7.45/four protons) indicated that the samples **P-30**, **P-45**, and **P-65** have 34%, 38%, and 8% of dopants in the nanomaterials, respectively. FT-IR analysis of the polyaniline nanomaterials (see the Supporting Information) showed two peaks at 3234 and 2920 cm^{-1} corresponding to −N−H and −C−H vibrations, respectively.[18] The peaks 1575, 1495, 1310, and 815 cm^{-1} were assigned to the quinoid ring C═C, benzenoid ring C═C

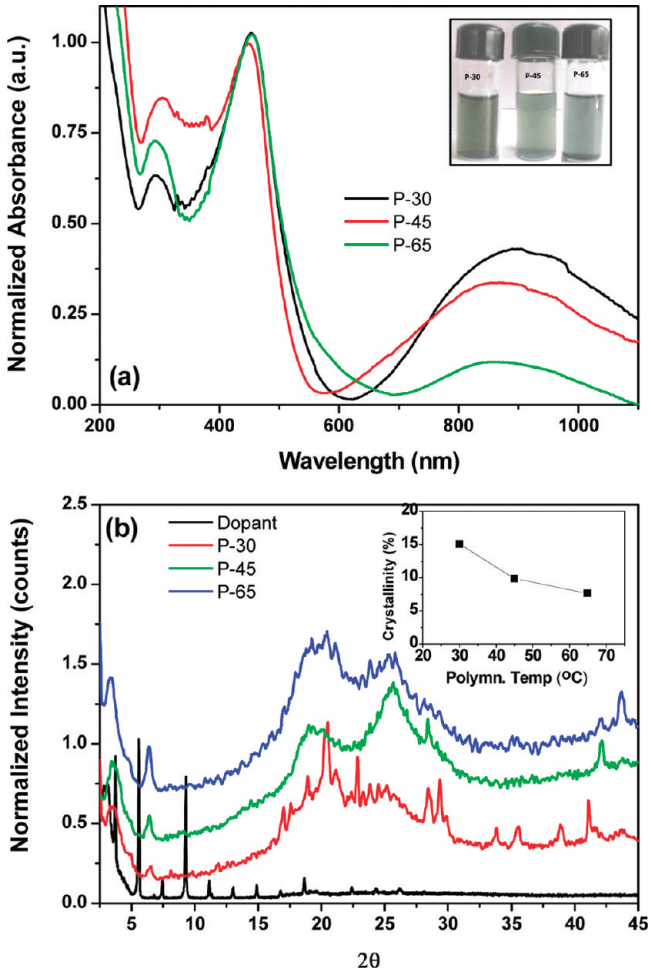

Figure 7. Absorption spectra and WXRD patterns of polyaniline nanomaterials.

stretching ring deformations, C−N stretching, and C−H out-of-plane vibrations of 1,4-disubstituted benzene ring, respectively.[19] The appearance of the peaks at 1300, ~630, and 1046 cm^{-1} was attributed to symmetric, unsymmetric stretching vibrations of $O{=}S{=}O$ and S−O groups and $NH^{+}\cdots SO_3^{-}$ interactions between the polymers chain and the dopant.[20] The inherent viscosity of the polymer nanofibers (in PANI-EB form) was determined for 0.5 wt % solutions in NMP at 30 °C. The inherent viscosities of the polymers were obtained in the range of $\eta_{inh} = 0.24-0.31$ dL/g. The viscosities of the samples indicate the formation of good molecular weight samples, and the values are similar to the earlier reports for polyaniline materials.[21]

The polyaniline nanostructures are water suspendable, and the solution is stable at ambient conditions. UV−vis spectra of the nanostructures were recorded in water, and they are shown in Figure 7a. The spectra of nanofibers contain all of the characteristic peaks of doped form of polyaniline emeraldine salt. The peaks at 310, 430, and 900 nm are assigned to the transitions of the $\pi-\pi^*$ band, polaron band to π^* band, and π band to polaron band, respectively.[22] Typically, polyaniline chains are expected to show a large difference in the peak intensities at 400 and 900 nm for expanded or coil-like conformations.[22] The tail-like nature and relatively low peak intensities at 900 nm (as compared to 400 nm) revealed that all of these polyaniline nanomaterials possessed expanded-like chain conformation. WXRD patterns of dopant gel and polyaniline nanomaterials are shown in Figure 7b. The polyaniline nanomaterials have sharp lower angle peaks at $2\theta = 3.4°$ (d-spacing = 25.6 Å) and at $2\theta = 6.4°$ (d-spacing = 13.7 Å). These peaks are assigned to layered structural organization of polyaniline chains followed by the interdigitations and crystallization of the dopant tails on the comb-shaped polyaniline chains.[23] Besides these peaks, there are broad peaks around $2\theta = 20°$ ($d = 4.6$ Å) and 25° ($d = 3.5$ Å), which are ascribed to aromatic $\pi-\pi$ interactions between stacks of phenylene rings present in the polymer chain and dopant, respectively. In all nanostructures, the 3.4° Bragg peak had a d-spacing value in the range of 25.6 Å, which is comparable to the end-to-end molecular length of 27.1 Å of the dopant molecule. This suggests that the polyaniline−dopant complex exhibited a lamellar-type structural organization in which stacks of polymer chains are separated by dopant sulfonate anions. In **P-30** nanofibers, the higher angle peaks are very sharp, and the amorphous hollow region is very much suppressed with respect to high crystallinity. The percent crystallinity of the polymer samples was determined by deconvolution of the WXRD peaks into sharp crystalline peaks and broad amorphous regions. The percent crystallinity of the samples **P-30**, **P-45**, and **P-65** was found to be 15.1%, 9.9%, and 7.7%, respectively (see inset of Figure 7b). This indicates that the gel-template stability is very important and crucial in manipulating the morphology as well as solid-state ordering of the polymer nanomaterials. The samples synthesized in the gel-state have much higher crystallinity as compared to those obtained from sol-state.

Typically, polyaniline nanomaterials are highly amorphous and do not show any transitions in thermal analysis. Interestingly, the polyaniline nanomaterials synthesized via the gel-assisted process possessed strong interactions between dopant and polyaniline, which enabled the thermal analysis by DSC. Polyaniline samples were heated from 223 to 473 K (−50 to 200 °C) and cooled from 473 to 223 K at a rate of 10 K/min to record their thermal transitions. DSC thermograms of dopant and polyaniline nanomaterials are given in Figure 8. The DSC plot of the dopant showed a sharp exothermic peak at 333 K ($\Delta H = 21.9$ J/g) corresponding to crystallization while cooling from the melt. On subsequent heating, two closely placed endothermic peaks at 348 K ($\Delta H = 32.2$ J/g) and 359 K ($\Delta H = 6.5$ J/g) were observed corresponding to the transitions from crystalline to melt. All three polymer samples showed multiple melting transitions in the first heating cycle. In the cooling cycle, samples **P-30** and **P-45** showed a sharp crystallization peak, except **P-65** did not (see the Supporting Information). The samples were subjected to annealing at 253 K (−20 °C) for more than 48 h and then subjected to DSC analysis for reproducible results. The heating/cooling cycles of annealed samples are shown in Figure 8 along with dopant. The thermograms of annealed samples were almost identical to that of the first heating/cooling experiments; however, their enthalpies are slightly different. The samples showed a broad endotherm in the region of 330−400 K during heating with a sharp peak at 379 K corresponding to the melting of the gel phase (in samples **P-30** and **P-45**). The enthalpies of melting transition for the annealed samples were obtained as 43.8, 22.2, and 17.2 J/g for **P-30**, **P-45**, and **P-65**, respectively. The more crystalline samples need higher energy for melting, and, therefore, the melting enthalpies were found in the order of **P-30** > **P-45** > **P-65**. Upon cooling, **P-30** and **P-45** showed crystallization peaks at 344 ($\Delta H = 0.6$ J/g) and 312 K ($\Delta H = 1.7$ J/g), respectively, whereas **P-65** failed to show any crystallization. DSC analysis confirmed that the samples **P-30** and **P-45**, which were synthesized in gel-state, possessed more crystallinity than **P-65**, which was obtained from the sol-state. The WXRD

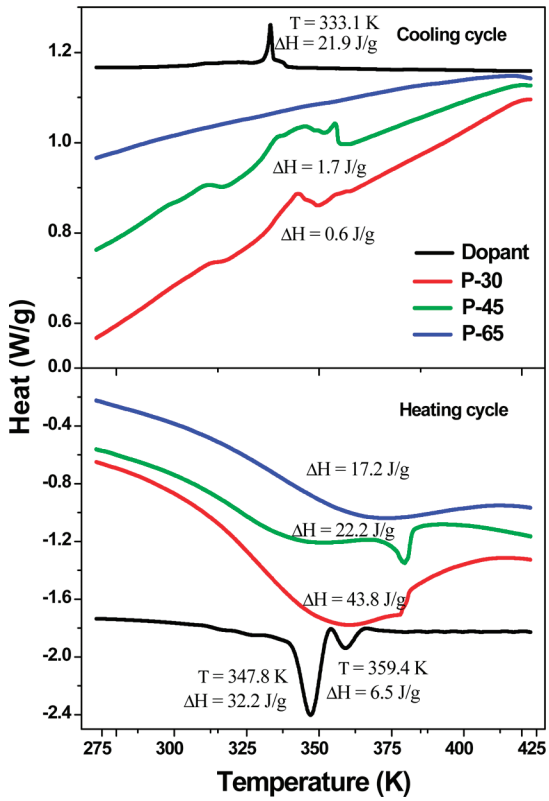

Figure 8. DSC thermograms of dopant and polyaniline nanomaterials.

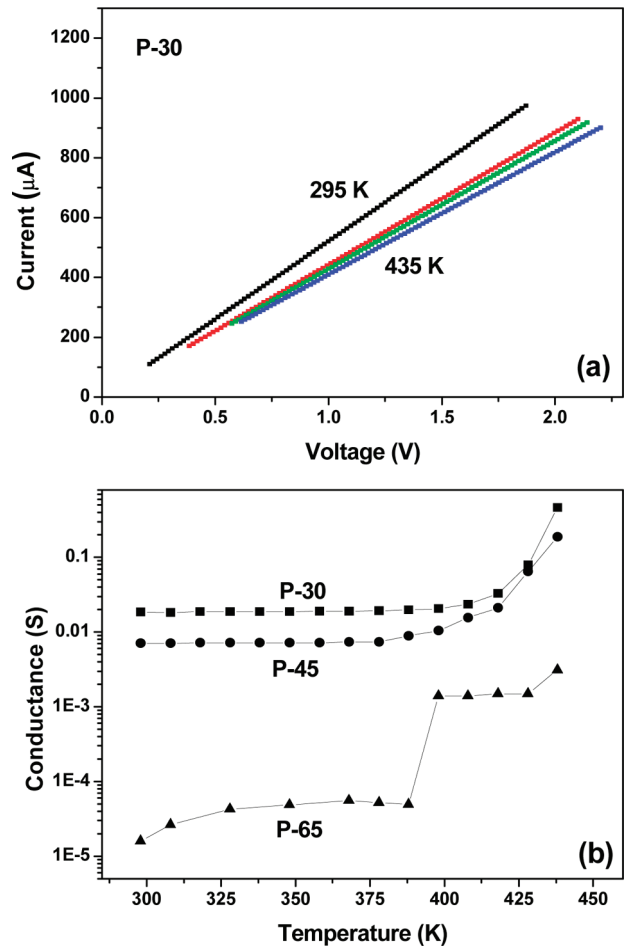

Figure 9. $I-V$ plot and conductance versus temperature plots of nanomaterials.

analysis (see Figure 7b) of the polymer samples also showed a similar trend of high percent crystallinity for samples prepared in gel-state (**P-30** and **P-45**) as compared to sol-state (**P-65**). This is clear evidence that in the gel-state polymerization route, the supramolecular interaction between the dopant molecules and polyaniline chain is retained in the nanofibrillar network for producing highly ordered and crystalline samples. On the other hand, the samples prepared in the sol-state (for **P-65**) are found to be amorphous due to the lack of dopant−polyaniline interactions.

Conducting nanomaterials are expected to show strong correlation between the solid-state ordering (crystallinity) and the electronic properties. To study the effect of gel-assisted self-organization on the electrical conductivity, the samples were subjected to temperature-dependent four-probe conductivity measurements for compressed pellets (see Figure 9). The linear trend in the current versus voltage ($I-V$) plots of the **P-30** and **P-65** (see Figure 9a) clearly showed that the polyaniline nanomaterials followed typical ohmic behavior.[24] The temperature versus the conductance was plotted for all three samples and shown in Figure 9b. At room temperature (300 K), the samples **P-30**, **P-45**, and **P-65** showed conductance of 0.02, 0.08, and 1.8×10^{-5} S, respectively. The difference in conductance among the samples was correlated to the difference in morphology, degree of doping, solid state % crystallinity, and enthalpies of thermal transitions (see Supporting Information). The sample **P-30** showed a higher $\Delta H = 43.8$ J/g (also % crystallinity) and has high conductivity, whereas amorphous sample **P-65** (less ΔH and % crystallinity) has 3 orders less conductance than ordered structures (**P-30** and **P-45**). The temperature-dependent conductance measurements revealed that there is a slight increase in the conductivity of the samples up to 400 K, but a huge jump of 2 orders in magnitude was observed above 410 K. The conductance reaches the maximum value of 0.45 and 0.21 for **P-30** and **P-45**, respectively. Yet the less ordered sample **P-65** still showed a less conductance of 3.3×10^{-3} S even at 450 K. It is interesting to note that the conductance increment occurs at a temperature just above the melting temperature of dopant−polyaniline complex obtained by DSC (380 K). We believe that upon heating the polymer fibrils become more flexible and better contact is established above 400 K, and the expanded state in turn improves the electrical conduction.

To study the electronic transport behavior of the material, the resistance of the material as a function of temperature was measured (see the Supporting Information). Over the temperature range of 298−438 K, the nanomaterials exhibited semiconducting behavior; that is, the resistance decreased with increasing temperature. In the insulating regime, the low-temperature resistivity $\rho(T)$ of the conducting polymer followed the exponential temperature dependence of variable range hopping (VRH):

$$\rho(T) = \rho_0 \exp(T_0/T)^m$$

where the exponent $m = 1/4$, 1/3, and 1/2 for three-dimensional (3D), two-dimensional (2D), and one-dimensional (1D) hopping, respectively.[25] T_0 is the Mott characteristic temperature and can be obtained from the slope of ln $R(T)$ versus $T^{-1/m}$ plot. Because bulk conductivity of the nanofibers follows conductivity like one-dimensional semiconductors, the ln R versus $T^{-1/2}$ is plotted. At temperatures below 400 K ($T^{-1/2} > 0.049$), there is no considerable change in ln R values, and therefore the data above 410 K ($T^{-1/2} < 0.049$) are used for the Motts plot. The plots

showed a linear trend and followed the VRH model. The T_0 values for **P-30**, **P-45**, and **P-65** were obtained as 1.57×10^3, 1.59×10^3, and 2.62×10^2 K, respectively, which are in accordance with earlier reports for metallic conductivity of polyaniline.[25] The ordered and crystalline nanomaterials synthesized in the gel-state showed almost 1 order difference in the Mott temperature as compared to that of the amorphous sample synthesized in the sol-state. The electrical conductance measurements revealed that the polyaniline nanomaterials exhibit linear current−voltage behavior corresponding to electronic conductivity (Ohm's law), and the conductance showed a temperature-dependent increment similar to a semiconductor following the 3-D VRH model at elevated temperatures.

Conclusion

We have successfully utilized the self-assembled gel formed by a new renewable resource-based amphiphilic sulfonic acid dopant to template polyaniline nanofibers. We have demonstrated the gel template has a pivotal role in directing polyaniline chains to form nanofibers. SEM, AFM, and TEM techniques have been successfully utilized to trace the nature and shape of polymerization templates to understand the mechanism of the nanomaterials formation. This novel gel template approach for polyaniline nanofibers has the following salient features: (i) a novel gel forming amphiphilic sulfonic acid dopant was developed from renewable resource-based 3-pentadecyl phenol, (ii) the dopant forms self-assembled opaque gels in highly polar organic solvents like aliphatic alcohols, chloroform, DMSO, etc., (iii) the gelation characteristics were studied by DSC and WXRD, (iv) SEM, AFM, and TEM analysis of dopant gels showed that the molecules are self-assembled into nanotubes, (v) the dopant molecules also self-assembled in the presence of aniline as gels with the aniline molecule preferentially trapped inside the nanotubes, (vi) this oxidation of gel-template produces polyaniline nanofibers, (vii) the polymerization at various temperatures clearly showed that the physical state and stability of the gel play a major role in determining the morphology, (viii) the nanomaterials showed high solubility in polar solvents like water and DMSO that enabled us to characterize these materials by NMR, UV−vis, FTIR, and cyclic voltammetry, (ix) WXRD and DSC analysis revealed that the samples synthesized at gel-state possessed highly crystalline as compared to that of sol-state samples, (x) the supramolecular interaction between dopant and polyaniline complex formed lamellae of interdigitated dopant molecules stacked between polyaniline chains and improved the solid-state properties, and (xi) the temperature-dependent conductance measurements showed a high conductivity of the gel-template synthesized samples, and they followed 3-D VRH model at elevated temperature. In a nut shell, we have shown for the first time that the novel amphiphilic dopant derived from renewable resource is a good gelator, and the gel assemblies are good template for the growth of highly ordered and soluble polyaniline nanofibers. The self-assisted organogel molecular template approach demonstrated here will open up new pathways in the design of well-defined conducting polymer nanomaterials.

Acknowledgment. We thank the Department of Science and Technology, New Delhi, India, for financial support under NSTI Programmes-SR/S5/NM-06/2007 and SR/NM/NS-42/2009. We thank Mr. M. R. Chandran, Dr. V. S. Prasad, Mr. Prasanth, Mr. P. Gurusamy, and Mr. Adarsh of NIIST-Trivandrum for SEM, TEM, AFM, WXRD, and NMR measurements. P. Anilkumar thanks UGC-New Delhi, India, for a senior research fellowship.

Supporting Information Available: ^{13}C NMR, mass, and gelation studies of dopant molecule and snapshot showing gel-assisted aniline polymerization. Thermogravimetric analysis (TGA), FTIR, UV−vis (dedoped), DSC (first heating), cyclic voltammogram (CV), and conductance (Motts plots) details of polyaniline nanomaterials. This material is available free of charge via the Internet at http://pubs.acs.org.

References and Notes

(1) (a) MacDiarmid, A. G. *Angew. Chem., Int. Ed.* **2001**, *40*, 2581–2590. (b) Hatchett, D. W.; Josowicz, M. *Chem. Rev.* **2008**, *108*, 746–769. (c) Alam, M. M.; Wang, J.; Guo, Y.; Lee, S. P.; Tseng, H. R. *J. Phys. Chem. B* **2005**, *109*, 12777–12784. (d) Haung, J.; Virji, S.; Kaner, R. B.; Weiller, B. H. *Nano Lett.* **2004**, *4*, 491–496. (e) Janata, J.; Josowicz, M. *Nat. Mater.* **2002**, *2*, 19–24. (f) Haung, J.; Virji, S.; Weiller, B. H.; Kaner, R. B. *Chem.-Eur. J.* **2004**, *10*, 1314.

(2) (a) Li, D.; Huang, J.; Kaner, R. B. *Acc. Chem. Res.* **2009**, *42*, 135–145. (b) Zhang, D. H.; Wang, Y. Y. *Mater. Sci. Eng., B* **2006**, *134*, 9–19. (c) Wan, M. X. *Adv. Mater.* **2008**, *20*, 2926–2932. (d) Tran, H. D.; Li, D.; Kaner, R. B. *Adv. Mater.* **2009**, *21*, 1–13. (e) Huang, J.; Kaner, R. B. *Chem. Commun.* **2006**, 367. (f) Wan, M. X. *Macromol. Rapid Commun.* **2009**, *30*, 963–975. (g) Zhang, X.; Goux, W. J.; Manohar, S. K. *J. Am. Chem. Soc.* **2004**, *126*, 4502–4503. (h) Chiou, N. R.; Epstein, A. J. *Adv. Mater.* **2005**, *17*, 1679–1683.

(3) (a) Zhang, Z.; Wei, Z.; Wan, M. X. *Macromolecules* **2002**, *35*, 5937–5942. (b) Wei, Z.; Zhnag, Z.; Wan, M. X. *Langmiur* **2002**, *18*, 917–921. (c) Zhang, L.; Wan, M. X. *Adv. Funct. Mater.* **2003**, *13*, 815–820. (d) Yan, Y.; Yu, Z.; Huang, Y. W.; Yuan, W. X.; Wei, Z. X. *Adv. Mater.* **2007**, *19*, 3353. (e) Hatano, T.; Bae, A. H.; Takeuchi, M.; Fujita, N.; Kaneko, K.; Ihara, H.; Takafuji, M.; Shinkai, S. *Chem.-Eur. J.* **2004**, *10*, 5067–5075.

(4) (a) Han, J.; Song, G.; Guo, R. *Adv. Mater.* **2007**, *19*, 2993. (b) Huang, L.; Wang, Z.; Wang, H.; Cheng, X.; Mitra, A.; Yan, Y. *J. Mater.Chem.* **2002**, *12*, 388–391. (c) Ryu, J.; Park, C. B. *Angew. Chem., Int. Ed.* **2009**, *48*, 1–5.

(5) (a) Anilkumar, P.; Jayakannan, M. *J. Phys. Chem. B* **2009**, *113*, 11614–11624. (b) Anilkumar, P.; Jayakannan, M. *Macromolecules* **2008**, *41*, 7706–7715. (c) Anilkumar, P.; Jayakannan, M. *Langmuir* **2008**, *24*, 9754–9762. (d) Anilkumar, P.; Jayakannan, M. *Macromolecules* **2007**, *40*, 7311–7319. (e) Anilkumar, P.; Jayakannan, M. *J. Phys. Chem. C* **2007**, *111*, 3591–3600. (f) Jinish Antony, M.; Jayakannan, M. *J. Phys. Chem. B* **2007**, *111*, 12772–12780. (g) Anilkumar, P.; Jayakannan, M. *Langmuir* **2006**, *22*, 5952–5957. (h) Jinish Antony, M.; Jayakannan, M. *J. Polym. Sci., Part B: Polym. Phys.* **2009**, *47*, 830–846. (i) Anilkumar, P.; Jayakannan, M. *J. Appl. Polym. Sci.* **2009**, *114*, 3531–3541.

(6) (a) Jung, J. H.; Lee, S. H.; Yoo, J. S.; Yoshida, K.; Shimizu, T.; Shinkai, S. *Chem.-Eur. J.* **2003**, *9*, 5307–5313. (b) Jia, Q.; Shimizu, T. *Chem. Commun.* **2005**, 4411–4413. (c) Ono, Y.; Nakashima, K.; Sano, M.; Hojob, J.; Shinkai, S. J. *J. Mater. Chem.* **2001**, *11*, 2412–2419. (d) Ji, Q.; Iwaura, R.; Shimizu, T. *Chem. Mater.* **2007**, *19*, 1329–1334. (e) Shimizu, T. *J. Polym. Sci., Part A: Polym. Chem.* **2006**, *44*, 5137–5152.

(7) (a) Vikki, T.; Pietila, L. O.; Osterholm, H.; Ahjopalo, L.; Takala, A.; Toivo, A.; Levon, K.; Passiniemi, P.; Ikkala, O. *Macromolecules* **1996**, *29*, 2945. (b) Jana, T.; Nandi, A. K. *Langmuir* **2000**, *16*, 3141. (c) Vecino, M.; Gonzalez, I.; Munoz, M. E.; Santamaria, A.; Pomposo, J. A. *Polymer* **2003**, *44*, 5057. (d) Jana, T.; Nandi, A. K. *Langmuir* **2001**, *17*, 5768. (e) Jana, T.; Chatterjee, J.; Nandi, A. K. *Langmuir* **2002**, *18*, 5720.

(8) (a) Meng, L.; Lu, Y.; Wang, X.; Zhang, J.; Duan, Y.; Li, C. *Macromolecules* **2007**, *40*, 2981–2983. (b) Li, G.; Zhang, Z. *Macromolecules* **2004**, *37*, 2683–2685. (c) Li, C.; Hatano, T.; Takeuchi, M.; Shinkai, S. *Chem. Commun.* **2004**, 2350–2351. (d) Tovar, J. D.; Rabatic, B. M.; Stupp, S. I. *Small* **2007**, *3*, 2024–2028.

(9) (a) John, G.; Masuda, M.; Okada, Y.; Yase, K.; Shimizu, T. *Adv. Mater.* **2001**, *13*, 715–718. (b) John, G.; Jung, J. H.; Minamikawa, H.; Yoshida, K.; Shimizu, T. *Chem.-Eur. J.* **2002**, *8*, 5494.

(10) (a) Deepa, P.; Jayakannan, M. *J. Polym. Sci., Part A: Polym. Chem.* **2007**, *45*, 2351–2366. (b) Rekha, N.; Asha, S. K. *J. Polym. Sci., Part A: Polym. Chem.* **2009**, *47*, 2996–3009.

(11) John, G.; Jung, J. H.; Masuda, M.; Shimizu, T. *Langmuir* **2004**, *20*, 2060–2065.

(12) McGrath, K. K.; Jang, K.; Robins, K. A.; Lee, D. C. *Chem.-Eur. J.* **2009**, *15*, 4070–4077.

(13) (a) Vemula, P. K.; John, G. *Acc. Chem. Res.* **2008**, *41*, 769–782. (b) Yui, H.; Guo, Y.; Koyama, K.; Sawada, T.; John, G.; Yang, B.; Masuda, M.; Shimizu, T. *Langmuir* **2005**, *21*, 721–727.

(14) Shimizu, T. *J. Polym. Sci., Part A: Polym. Chem.* **2008**, *46*, 2601–2611.

(15) (a) Jana, T.; Roy, S.; Nandi, A. K. *Synth. Met.* **2003**, *132*, 257. (b) Kosonen, H.; Ruokolainen, J.; Knaapila, M.; Torkkeli, M.; Jokela, K.;

Serimaa, R.; ten Brinke, G.; Bras, W.; Monkman, A. P.; Ikkala, O. *Macromolecules* **2000**, *33*, 8671.

(16) Goto, H.; Akagi, K. *Macromolecules* **2002**, *35*, 2545–2551.

(17) (a) Zhou, C.; Han, J.; Song, G.; Guo, R. *J. Polym. Sci., Part A: Polym. Chem.* **2008**, *46*, 3563. (b) Mu, S.; Yang, Y. *J. Phys. Chem. B* **2008**, *112*, 11558.

(18) (a) Zheng, W.; Angelopoulos, M.; Epstein, A. J.; MacDiarmid, A. G. *Macromolecules* **1997**, *30*, 7634–763. (b) Zheng, W.; Angelopoulos, M.; Epstein, A. J.; MacDiarmid, A. G. *Macromolecules* **1997**, *30*, 2953–2955.

(19) (a) Kang, E. T.; Neoh, K. G.; Tan, K. L. *Prog. Polym. Sci.* **1998**, *23*, 211–324. (b) Li, X. G.; Wang, H. Y.; Huang, M. R. *Macromolecules* **2007**, *40*, 1489–1496.

(20) Jayakannan, M.; Anilkumar, P.; Sanju, A. *Eur. Polym. J.* **2006**, *42*, 2623–2631.

(21) (a) Kim, B. J.; Oh, S. G.; Han, M. G.; Im, S. S. *Synth. Met.* **2001**, *122*, 297–304. (b) Erdem, E.; Karakısla, M.; Sacak, M. *Eur. Polym. J.* **2004**, *40*, 785–791. (c) Jayakannan, M.; Annu, S.; Ramalekshmi, S. *J. Polym. Sci., Part B: Polym. Phys.* **2005**, *43*, 1321.

(22) (a) Xis, Y.; Wiesinger, J. M.; MacDiarmid, A. G. *Chem. Mater.* **1995**, *7*, 443–445. (b) MacDiarmid, A. G.; Epstein, A. J. *Synth. Met.* **1995**, *69*, 85–92.

(23) (a) Dufour, B.; Rannou, P.; Fedorko, P.; Djurado, D.; Travers, J. P.; Pron, A. *Chem. Mater.* **2001**, *13*, 4032–4040. (b) Laska, J.; Djurado, D.; Lunzy, W. *Eur. Polym. J.* **2002**, *38*, 947–951. (c) Lunzy, W.; Banka, E. *Macromolecules* **2000**, *33*, 425.

(24) (a) Long, Y.; Chen, Z.; Ma, Y.; Zhang, Z.; Jin, A.; Gu, C.; Zhang, L.; Wei, Z.; Wan, M. X. *Appl. Phys. Lett.* **2004**, *84*, 2205–2207. (b) Mativetsky, J. M.; Datars, W. R. *Physica B* **2002**, *324*, 191–204. (c) Adetunji, O. O.; Chiou, N. R.; Epstein, A. J. *Phys. Rev. B* **2009**, *80*, 12201–12204.

(25) (a) Long, Y.; Chen, Z.; Wang, N.; Ma, Y.; Zhang, Z.; Zhang, L.; Wan, M. X. *Appl. Phys. Lett.* **2003**, *83*, 1864–1865. (b) Long, Y.; Chen, Z.; Zheng, P.; Wang, N.; Zhang, Z.; Wan, M. X. *J. Appl. Phys.* **2003**, *93*, 2962–2965. (c) Long, Y.; Zhang, L.; Ma, Y.; Chen, Z.; Wang, N.; Zhang, Z.; Wan, M. X. *Macromol. Rapid Commun.* **2003**, *24*, 938–942.

JP909016R